Molecular-frame differential photoelectron circular dichroism of O 1s-photoelectrons of trifluoromethyloxirane

G. Nalin,[1] N. M. Novikovskiy,[2] K. Fehre,[1] N. Anders,[1] D. Trabert,[1] S. Grundmann,[1] M. Kircher,[1] A. Khan,[1] R. Tomar,[1] M. Hofmann,[1] M. Waitz,[1] I. Vela-Perez,[1] G. Kastirke,[1] J. Siebert,[1] D. Tsitsonis,[1] C. Küstner-Wetekam,[2] L. Marder,[2] J. Viehmann,[2] F. Trinter,[3,4] H. Fukuzawa,[5] K. Ueda,[5] J. B. Williams,[6] A. Knie,[2] R. Dörner,[1] M. S. Schöffler,[1] T. Jahnke,[7] and Ph. V. Demekhin[2,*]

[1]*Institut für Kernphysik, Goethe-Universität, Max-von-Laue-Straße 1, 60438 Frankfurt am Main, Germany*
[2]*Institut für Physik und CINSaT, Universität Kassel, Heinrich-Plett-Straße 40, 34132 Kassel, Germany*
[3]*Deutsches Elektronen-Synchrotron (DESY), Notkestraße 85, 22607 Hamburg, Germany*
[4]*Molecular Physics, Fritz-Haber-Institut der Max-Planck-Gesellschaft, Faradayweg 4-6, 14195 Berlin, Germany*
[5]*Institute of Multidisciplinary Research for Advanced Materials, Tohoku University, Sendai 980-8577, Japan*
[6]*Department of Physics, University of Nevada, Reno, Nevada 89557, USA*
[7]*European XFEL GmbH, Holzkoppel 4, 22869 Schenefeld, Germany*

(Received 10 September 2022; accepted 12 December 2022; published 17 January 2023)

The differential photoelectron circular dichroism (PECD) of O 1*s* photoelectrons of *R*-trifluoromethyloxirane enantiomers as a function of the photoelectron emission direction in the molecular frame of reference and the direction from which circularly polarized light hits the molecule, is studied experimentally and theoretically for different photoelectron kinetic energies. A coincident detection of the photoelectrons and two ionic molecular fragments, performed with cold target recoil ion momentum spectroscopy, allows us to determine the orientation of the molecule in the laboratory frame and to obtain in addition the molecular-frame photoelectron diffraction patterns. From these we deduce the differential PECD. For given molecular orientations and photoelectron emission directions, we observe a normalized PECD strength clearly beyond 50%. These observations are in agreement with respective relaxed-core Hartree-Fock calculations, performed by employing the single center method. The present results support our recent observation of a huge differential PECD in O 1*s* photoemission of the methyloxirane molecule.

DOI: 10.1103/PhysRevResearch.5.013021

I. INTRODUCTION

Since its experimental verification [1], photoelectron circular dichroism (PECD, [2]) attracted considerable attention from both experimental and theoretical sides (see, e.g., review articles Refs. [3–6]). The effect manifests as a substantial laboratory-frame forward-backward asymmetry in the emission of photoelectrons from chiral molecules (typically on the order of a few percent of the total ionization signal), which can be explained within the electric-dipole approximation. Because its relative strength is much larger than that of a conventional circular dichroism [7], and owing to its universality with respect to the photoionization regime [8,9], PECD has become nowadays an extremely sensitive [10] laboratory tool for chiral recognition in the gas phase.

The PECD of randomly oriented molecules is characterized by the odd coefficients in the expansion of the laboratory-frame differential photoionization cross section over Legendre polynomials [11–13]. Those expansion coefficients are differential quantities, which result from an incomplete compensation between different partial photoionization amplitudes [2]. Thus, for randomly oriented molecules, the effect partially cancels out leading to a much reduced signal strength. On the contrary, a circular dichroism in the angular distribution [14,15] and even an *apparent* PECD [16] on the order of 100% can be observed when fixing *achiral* diatomic molecules in space. Thus, as predicted theoretically in our previous work [17], PECD becomes an effect as strong as 100% when certain (fixed) orientations of chiral molecules with respect to the propagation direction of the ionizing light are considered. Such a huge dichroic contrast considerably increases the sensitivity of PECD, e.g., for enantiomeric-excess determination.

In order to confirm this prediction, we first studied in the past uniaxially oriented chiral molecules. As test bench systems, we chose methyloxirane (MOx, C_3H_6O) in Ref. [17] and trifluoromethyloxirane (TFMOx, $C_3H_3F_3O$) in Refs. [18,19]. These joint experimental and theoretical studies [17–19] confirmed that fixing already one molecular orientation axis in space increases the differential PECD by almost an order of magnitude. In a subsequent study of MOx, we were able to finally perform measurements of a chiral molecule fully fixed in space and reported enantiosensitive polarization-averaged

*demekhin@physik.uni-kassel.de

molecular-frame photoelectron diffraction patterns [20]. Very recently, we demonstrated a fourfold differential PECD of fully fixed-in-space MOx clearly beyond 50% [21], confirming thereby theoretical predictions of Ref. [17].

This article is part of our series of studies [18,19] of angle-resolved photoionization of TFMOx. Here, we investigate its differential PECD in the molecular frame of reference, similar to our previous studies of MOx [20,21]. In particular, we report the polarization-averaged molecular-frame and fourfold differential photoemission patterns with the respective PECDs for O 1*s* photoelectrons of TFMOx at different kinetic energies.

II. RESEARCH METHODS

A. Experiment

The experimental data for the O 1*s* photoionization of TFMOx were recorded at Synchrotron SOLEIL (Saint-Aubin, France) at beamline SEXTANTS using cold target recoil ion momentum spectroscopy (COLTRIMS, [22–24]) during the same experimental campaign as the data presented in Ref. [18]. The details on the experiment can be found therein. Briefly, the measurements were performed using enantiopure *R*-TFMOx molecules obtained commercially from SynQuest Laboratories. The molecular gas jet was introduced in the reaction chamber via expansion of the molecular vapor using a closed-loop recycling system [25]. The emitted electrons and ionic fragments were accelerated to opposite directions towards time- and position-sensitive microchannel-plate detectors with enhanced efficiency on the ion detector [26]. We employed a mesh-free COLTRIMS spectrometer with electrostatic lenses and (quasi) field-free drift regions. From the measured particles' positions of impact and times of flight, we reconstructed their initial vector momenta. The electron energy was calibrated via separate calibration measurements of Ar 2*p* photoelectrons. The measurements on TFMOx were performed at five selected photon energies, which yielded O 1*s* photoelectrons centered at kinetic energies of 3.1, 4.1, 6.1, 8.1, and 11.7 eV, respectively.

The measured momenta of the photoelectrons and ionic fragments provide the information on the spatial orientation of the molecule at the instant of the photoionization and allow thereby to access the photoelectron emission distributions in the molecular frame of reference (under the assumption of the axial-recoil approximation [27]). In more detail, we determined the spatial orientation of the individual TFMOx molecules in the gas phase by using the following fragmentation channel: $C_3H_3F_3O + \hbar\omega \rightarrow CF_3^+ + C_2H_2^+ + OH^0 + e^-_{\rm ph} + e^-_{\rm Aug}$. For this channel, we recorded between 3×10^5 and 6×10^5 valid events for each light helicity and photon energy. The neutral fragment was not recorded by our ion detection. Instead, we reconstructed the momentum vector of the neutral OH^0 fragment by using the measured momenta of the charged fragments and exploiting momentum conservation (while neglecting the recoil from the electrons and the linear momentum of the photon). In order to distinguish this fragmentation channel from background and to ensure that three fragment momenta define a plane (i.e., are not collinear), the following momentum gates were used: 70 a.u. $< |\vec{p}_{CF_3^+}| <$ 120 a.u., 80 a.u. $< |\vec{p}_{C_2H_2^+}| <$ 130 a.u., and 10 a.u. $< |\vec{p}_{OH^0}| <$ 35 a.u. The *fragment* coordinate system was constructed as $\vec{Y} = \vec{p}_{CF_3^+}$, $\vec{Z} = \vec{p}_{CF_3^+} \times \vec{p}_{C_2H_2^+}$, and $\vec{X} = \vec{Y} \times \vec{Z}$. The momenta of all fragments and the derived *fragment* coordinate system are schematically depicted in Fig. 1.

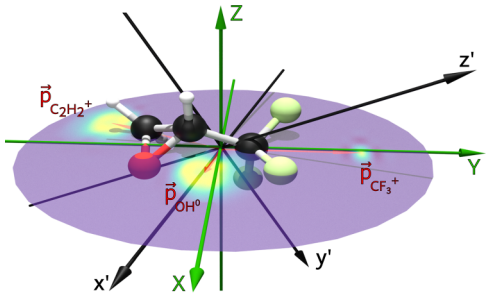

FIG. 1. The *fragment* coordinate system (green $\{X, Y, Z\}$ axes) for *R*-TFMOx, obtained with the help of the fragments' momenta (red arrows with yellow spots at their tips representing measured distributions), together with the constructed *molecular* coordinate system that corresponds to the instant of photoionization (black $\{x', y', z'\}$ axes, see the text for details).

B. Theory

The molecular-frame photoelectron angular distribution (MFPAD), induced by the one-photon ionization of a molecule using circularly polarized light ($q = \pm 1$), can be described by the following expansion of the differential photoionization cross section over (complex conjugated) spherical harmonics Y_{LM}:

$$\frac{d\sigma^q}{d\Omega_{\hat{\mathbf{k}}}}(\alpha, \beta; \theta, \phi) = \sum_{LM} B^q_{LM}(\alpha, \beta) Y^*_{LM}(\theta, \phi). \tag{1}$$

Here, $\hat{\mathbf{k}} = \{\theta, \phi\}$ are the photoelectron emission angles in the molecular frame of reference, and $\{\alpha, \beta\}$ are the Euler angles describing the orientation of that molecular coordinate frame with respect to the light propagation direction. Note that the third angle γ, which describes the rotation around the light propagation direction (laboratory z axis), is irrelevant for circularly polarized light and can be set to $\gamma = 0$. The remaining orientation angles can also be considered as polar β and azimuthal α spherical angles, describing the direction from which incident light hits the molecule.

The analytic expression for the expansion coefficients B^q_{LM} in Eq. (1) reads

$$\begin{aligned} B^q_{LM}(\alpha, \beta) = \sum_{\ell m k} \sum_{\ell' m' k'} & i^{(\ell+\ell')} (-1)^{\ell+m'} \\ & \times \sqrt{\frac{(2\ell+1)(2\ell'+1)(2L+1)}{4\pi}} \\ & \times \begin{pmatrix} \ell & \ell' & L \\ 0 & 0 & 0 \end{pmatrix} \begin{pmatrix} \ell & \ell' & L \\ m & -m' & M \end{pmatrix} \\ & \times \mathcal{D}^1_{kq}(\alpha, \beta) \mathcal{D}^{1*}_{k'q}(\alpha, \beta) A_{\varepsilon \ell m k} A^*_{\varepsilon \ell' m' k'}, \end{aligned} \tag{2}$$

where $\mathcal{D}$ are the Wigner rotation matrices. The photoelectron scattering phase $e^{-i\delta_{\ell m}}$ is included in the photoionization

transition amplitude $A_{\varepsilon\ell mk}$ for the emission of a photoelectron partial wave with energy ε, angular momentum ℓ, and its projection m, after absorption of a photon with polarization k, altogether given in the frame of molecular reference.

The simplest way to obtain polarization-averaged molecular-frame photoelectron angular distributions (PA-MFPADs) is to average over all molecular orientation Euler angles (i.e., by averaging over all possible directions of the ionizing light), which can be performed analytically using the following orthogonality properties of the rotational matrices:

$$\frac{1}{8\pi^2}\int d^3(\alpha\beta\gamma)\mathcal{D}^1_{kq}\mathcal{D}^{1*}_{k'q} = \frac{\delta_{kk'}}{3}. \tag{3}$$

As a consequence, the corresponding expansion coefficients B_{LM} become independent of the light polarization q [20]. The partial transition amplitudes $A_{\varepsilon\ell mk}$ for the O 1s photoionization of R-TFMOx, entering Eq. (2), were computed for the equilibrium internuclear geometry of the neutral electronic ground state with the single center (SC) method and code [28–30]. Calculations were performed in the relaxed-core Hartree-Fock approximation using the SC expansions restricted by $\ell_c \leqslant 79$ and $\ell_\varepsilon \leqslant 29$ for the occupied and continuum orbitals, respectively, as described in detail in our previous work on the O 1s photoionization of this molecule [18].

III. RESULTS AND DISCUSSION

A. Polarization-averaged MFPAD

In the case of a molecular breakup into fragments consisting of several atoms (where usually the fragments' center of mass does not coincide with the center of charge), the fragmentation dynamics is accompanied by relative rotations of the fragments. Thereby, the detected asymptotic momenta (see Fig. 1) and the *fragment* coordinate system $\{X, Y, Z\}$ derived from them cannot be related to the orientation of the molecule at the instant of photoemission in a straightforward manner. In order to infer such a *molecular* coordinate system $\{x', y', z'\}$, we applied a procedure introduced in our previous work [20]. In particular, we search for a molecular orientation, which provides the best agreement between the computed and the measured PA-MFPADs. For this purpose, first, the minimum value of each PA-MFPAD was subtracted from the distribution, and the integral emission signal was normalized to unity. We then quantified the amount of agreement between the renormalized theoretical $I_T(\theta, \varphi)$ and experimental $I_E(\theta, \varphi)$ emission patterns, using the following figure of merit,

$$d_2 = \sqrt{\iint [I_E(\theta, \varphi) - I_T(\theta, \varphi, \mathbf{R})]^2 d^2(\theta\varphi)}. \tag{4}$$

This parameter depends on the relative orientation of the *molecular* $\{x', y', z'\}$ and *fragment* $\{X, Y, Z\}$ coordinate systems, which is given by the roll, pitch, and yaw angles: $\mathbf{R} = \{R_X, R_Y, R_Z\}$. Based on the axial-recoil approximation [27] and using the assumption that the *molecular* and *fragment* coordinate systems coincide for the initial parameter, we computed the PA-MFPAD and, by rotating this computed pattern in small steps, searched for a molecular orientation that yields smallest values of d_2.

The procedure described above was applied to the data obtained for all five photoelectron kinetic energies and yielded very similar *molecular* coordinate systems, after applying this optimization scheme. This corresponding coordinate system is illustrated in Fig. 1 by the black $\{x', y', z'\}$ arrows. As one can see, this *molecular* coordinate system is considerably skewed with respect to the *fragment* coordinate system (depicted by the green $\{X, Y, Z\}$ arrows), suggesting strong (yet deterministic) relative rotation of the fragments in the course of this breakup. We observed a very similar result in our previous study on O 1s photoelectrons of uniaxially oriented TFMOx [18]. There, owing to intricate rotations of two fragments with respect to each other occurring in the course of a slow dissociation, a fragmentation axis (which connected the trifluoromethyl-group and oxirane-ring fragments) deviated from a theoretically found optimal axis (which was almost parallel to the plane of the oxirane ring).

The PA-MFPADs of the O 1s photoelectrons of R-TFMOx are depicted in Fig. 2 for five photoelectron kinetic energies as functions of the photoelectron emission angles. For the experiment, those angles are defined in the *fragment* coordinate system, and for theory, in the *molecular* system. As one can see from this figure, the theory provides a good semiquantitative description of the experiment, in particular, when considering the complexity of the problem. It is worth noting that the *fragment* coordinate system alone does not provide access to the handedness of the molecule. This is because the measured momenta of the fragments define only a plane. However, PA-MFPADs are enantiosensitive objects [20] and switching between the enantiomers mirrors the emission distributions via reflection at $\cos\theta = 0$.

B. Differential MFPADs and PECDs

We divided our data set with respect to the orientation of the molecule. Considering the available statistics recorded in the experiment, we binned that division in constant steps of $\Delta\cos\theta = \frac{1}{3}$ and $\Delta\varphi = 30^\circ$ into 72 subsets. We present these distributions as functions of the two photoelectron emission angles $\{\theta, \varphi\}$ and transformed the photon propagation direction into the same coordinates. Accordingly, the photoemission and light-propagation directions are defined in the *fragment* coordinate system for the experimental data and in the *molecular* system for the theoretical ones, just as in the preceding sections. However, for clarity, we will focus in the following on measured and computed MFPADs and PECDs for one representative molecular orientation, whereas the full set of results can be found in the Supplemental Material document [31].

The measured and computed MFPADs of the O 1s photoelectrons of R-TFMOx are depicted in Fig. 3 for five photoelectron kinetic energies. The experimental results are shown in the left column, the computed MFPADs on the right. These are the distributions highlighted by the red-colored border in the overview Figs. S1–S5 in the Supplemental Material [31]. The selected representative orientation of the molecule with respect to the propagation direction of circularly polarized light (negative helicity) is indicated in the bottom

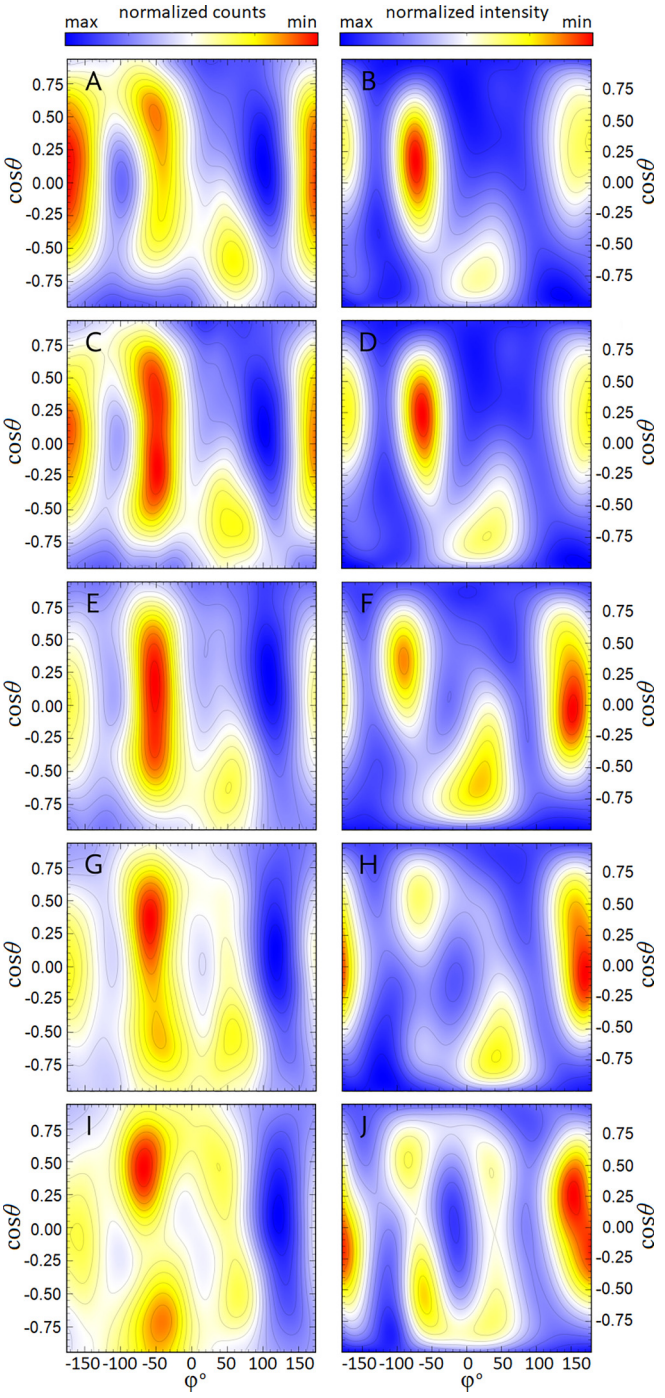

FIG. 2. Experimental (left panels A, C, E, G, and I) and theoretical (right panels B, D, F, H, and J) polarization-averaged molecular-frame photoelectron angular distributions (PA-MFPADs) as functions of the photoelectron emission angles $\{\theta, \phi\}$ for different kinetic energies of the O 1*s* photoelectrons of *R*-TFMOx. Panels A and B for 3.1 eV; C and D for 4.1 eV; E and F for 6.1 eV; G and H for 8.1 eV; I and J for 11.7 eV.

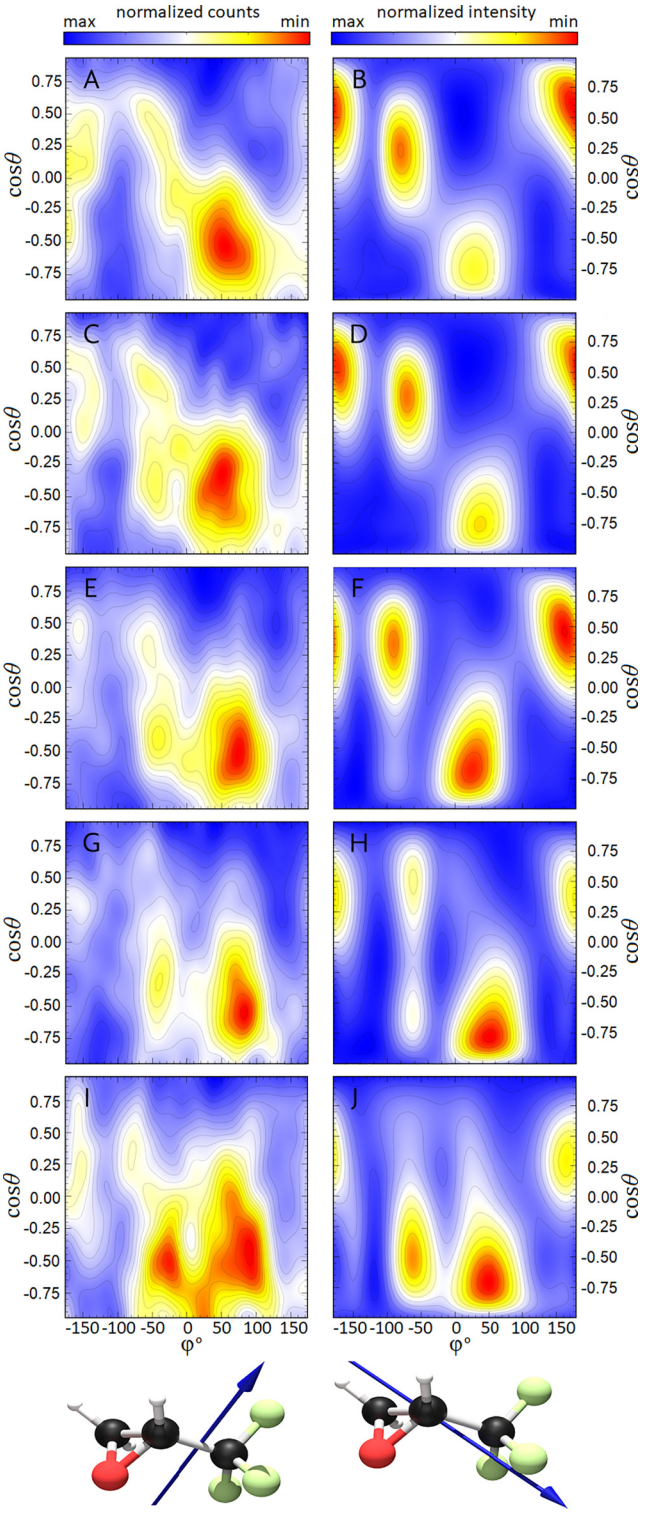

FIG. 3. Experimental (left panels A, C, E, G, and I) and theoretical (right panels B, D, F, H, and J) MFPADs as functions of the photoelectron emission angles $\{\theta, \phi\}$, obtained for different kinetic energies of the O 1*s* photoelectrons of *R*-TFMOx. The selected orientation of the molecule (with respect to the propagation direction of the circularly polarized light with negative helicity) is visualized at the bottom. This direction differs in the *fragment* and *molecular* coordinate systems (see the text for details). The photoelectron energy is 3.1 eV in panels A and B; 4.1 eV in C and D; 6.1 eV in E and F; 8.1 eV in G and H; 11.7 eV in I and J.

of Fig. 3. The relative skew between the *fragment* and the *molecular* coordinate systems, seen from those insets with respect to the light propagation direction, provides an estimate for the relative rotation of the fragments, which occurs during

the breakup of the molecule and prior to the detection of the fragments.

As one can see from this figure, the measured and computed differential MFPADs are in a reasonable semiquantitative agreement. In order to obtain such MFPADs for the opposite enantiomer (not measured in this paper) and light polarization, the following two symmetry operations (based on the electric-dipole approximation) can be used. First, the reflection of the photoelectron-emission and light-propagation coordinates at $\cos\,\theta = 0$ mediates simultaneous switching between the two enantiomers and the light helicities. Second, keeping the enantiomer and swapping helicity is equivalent to reversing the light propagation direction, which is mediated by transforming $\varphi \rightarrow \varphi + 180^\circ$ and $\cos\,\theta \rightarrow -\cos\,\theta$.

Similar to our previous works [17–19,21], the differential PECD is defined as the normalized difference of the photoelectron distributions recorded for circularly polarized light with positive and negative helicities (I_+ and I_-, respectively),

$$\mathrm{PECD}(\theta, \varphi) = \frac{I_+(\theta, \varphi) - I_-(\theta, \varphi)}{I_+(\theta, \varphi) + I_-(\theta, \varphi)}, \tag{5}$$

which corresponds to the half of the usually used $2b_1$ value [11–13]. The measured and computed differential PECDs of the O 1*s* photoelectrons of *R*-TFMOx are depicted in Fig. 4 for five photoelectron kinetic energies. The orientation of the molecule with respect to the light propagation direction is the same as in Fig. 3. The present theoretical predictions reproduce the measured PECD landscapes including their signs. However, the contrast of the computed PECDs (clearly above ±80%) is somewhat larger than that of the measured ones (which is only around ±50%).

IV. SUMMARY

The work presented in this paper is a logical continuation of our previous experimental and theoretical studies of the differential PECD of partly and fully fixed-in-space chiral molecules [17–21]. Here, we explored the differential PECD of O 1*s* photoelectrons in body-fixed-frame *R*-TFMOx molecules. In particular, we measured and computed the PA-MFPADs and the MFPADs of spatially oriented TFMOx for five photoelectron kinetic energies. In order to achieve a reasonable agreement between the present theory and the experiment, a substantial rotation of the fragments during the respective breakup was assumed. Thereby, the main emission patterns, observed in the experimental MFPADs of fixed-in-space TFMOx, are reproduced in the theory at similar photoelectron emission directions but still with a somewhat higher relative contrast. The found average skewing between the theoretically and experimentally deduced *molecular* and *fragment* coordinate frames, respectively, can be used to estimate the dynamics and times of a relative rotation of the fragments during the considered breakup. Possible reasons for a quantitative disagreement between the measured and computed MFPADs are discussed in great detail in our previous work on this molecule [18]. With the help of those MFPADs, we observe a differential PECD of fully fixed-in-space TFMOx molecules well beyond 50%, similar to our recent analogous study of the closely related molecule MOx [21]. Our studies confirm again that orienting the molecule increases the dichroic contrast of this chiral asymmetry by up to two orders of magnitude (from a few to almost 100%), which considerably improves its sensitivity for chiral recognition in the gas phase.

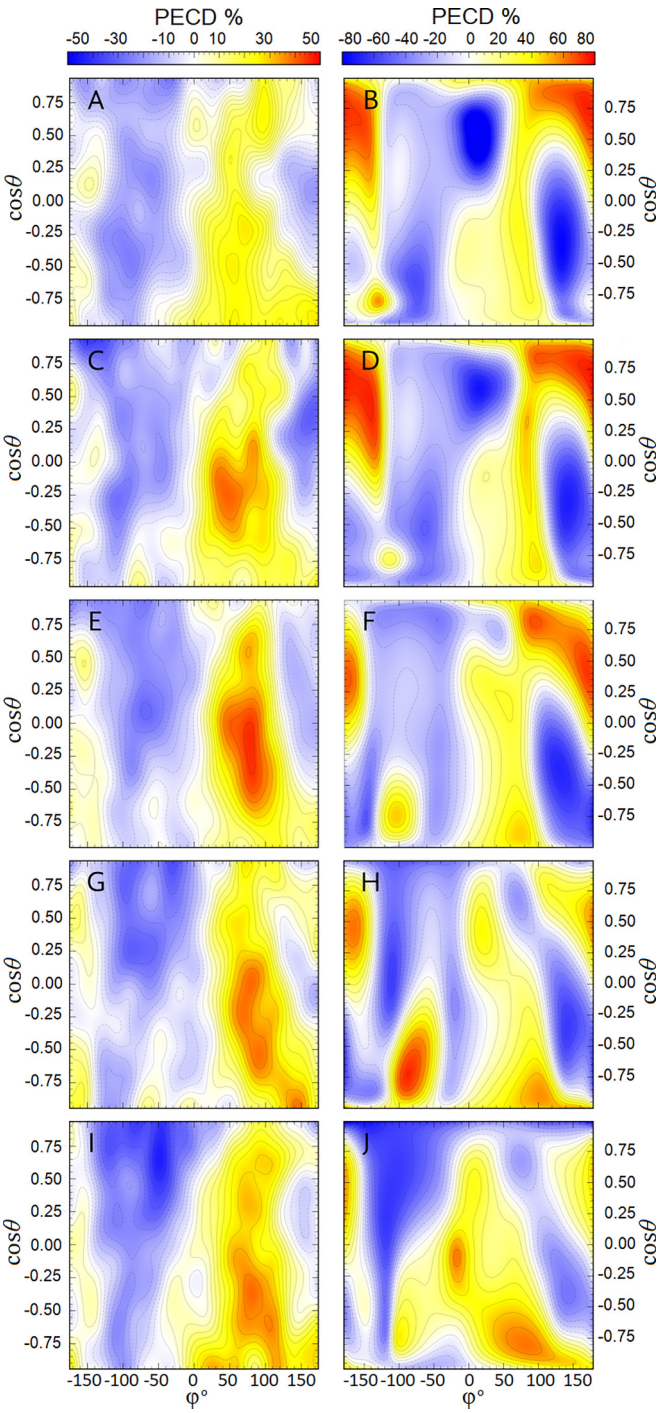

FIG. 4. Experimental (left panels A, C, E, G, and I) and theoretical (right panels B, D, F, H, and J) molecular-frame differential PECDs as functions of the photoelectron emission angles $\{\theta, \phi\}$, obtained for different kinetic energies of the O 1*s* photoelectrons of *R*-TFMOx. The molecular orientation with respect to the light propagation direction is the same as in Fig. 3. The photoelectron energy is 3.1 eV in panels A and B; 4.1 eV in C and D; 6.1 eV in E and F; 8.1 eV in G and H; 11.7 eV in I and J.

ACKNOWLEDGMENTS

This work was funded by the Deutsche Forschungsgemeinschaft (DFG)—Project No. 328961117–SFB 1319 ELCH (Extreme light for sensing and driving molecular chirality). This research was also undertaken as part of the ASPIRE Innovative Training Network, which has received funding from the European Union's Horizon 2020 Research and innovation Programme under the Marie Sklodowska-Curie Grant Agreement No. 674960. H.F. and K.U. acknowledge the XFEL Priority Strategy Program of MEXT, the Research Program of "Dynamic Alliance for Open Innovations Bridging Human, Environment and Materials" and the IMRAM Project for support. K.F. acknowledges support by the German National Merit Foundation. M.S.S. thanks the Adolf-Messer Foundation for financial support. We thank the staff of Synchrotron SOLEIL for running the facility and providing beam time under Project No. 20180746 and beamline SEXTANTS for excellent support.

[1] N. Böwering, T. Lischke, B. Schmidtke, N. Müller, T. Khalil, and U. Heinzmann, Asymmetry in Photoelectron Emission from Chiral Molecules Induced by Circularly Polarized Light, Phys. Rev. Lett. **86**, 1187 (2001).

[2] B. Ritchie, Theory of the angular distribution of photoelectrons ejected from optically active molecules and molecular negative ions, Phys. Rev. A **13**, 1411 (1976).

[3] I. Powis, Photoelectron circular dichroism in chiral molecules, Adv. Chem. Phys. **138**, 267 (2008).

[4] L. Nahon, G. A. Garcia, and I. Powis, Valence shell one-photon photoelectron circular dichroism in chiral systems, J. Electron Spectrosc. Relat. Phenom. **204**, 322 (2015).

[5] S. Turchini, Conformational effects in photoelectron circular dichroism, J. Phys.: Condens. Matter **29**, 503001 (2017).

[6] R. Hadidi, D. K. Bozanic, G. A. Garcia, and L. Nahon, Electron asymmetries in the photoionization of chiral molecules: possible astrophysical implications, Adv. Phys. X **3**, 1477530 (2018).

[7] N. Berova, K. Nakanishi, and R. W. Woody, *Circular Dichroism: Principles and Applications* (Wiley, New York, 2009).

[8] S. Beaulieu, A. Ferré, R. Géneaux, R. Canonge, D. Descamps, B. Fabre, N. Fedorov, F. Légaré, S. Petit, T. Ruchon, V. Blanchet, Y. Mairesse, and B. Pons, Universality of photoelectron circular dichroism in the photoionization of chiral molecules, New J. Phys. **18**, 102002 (2016).

[9] M. Wollenhaupt, Photoelectron circular dichroism in different ionization regimes, New J. Phys. **18**, 121001 (2016).

[10] A. Kastner, C. Lux, T. Ring, S. Züllighoven, C. Sarpe, A. Senftleben, and T. Baumert, Enantiomeric excess sensitivity to below one percent by using femtosecond photoelectron circular dichroism, ChemPhysChem **17**, 1119 (2016).

[11] C. S. Lehmann, N. B. Ram, I. Powis, and M. H. M. Janssen, Imaging photoelectron circular dichroism of chiral molecules by femtosecond multiphoton coincidence detection, J. Chem. Phys. **139**, 234307 (2013).

[12] M. H. M. Janssen and I. Powis, Detecting chirality in molecules by imaging photoelectron circular dichroism, Phys. Chem. Chem. Phys. **16**, 856 (2014).

[13] C. Lux, M. Wollenhaupt, C. Sarpe, and T. Baumert, Photoelectron circular dichroism of bicyclic ketones from multiphoton ionization with femtosecond laser pulses, ChemPhysChem **16**, 115 (2015).

[14] R. L. Dubs, S. N. Dixit, and V. McKoy, Circular Dichroism in Photoelectron Angular Distributions from Oriented Linear Molecules, Phys. Rev. Lett. **54**, 1249 (1985).

[15] T. Jahnke *et al.*, Circular Dichroism in K-Shell Ionization from Fixed-in-Space CO and N_2 Molecules, Phys. Rev. Lett. **88**, 073002 (2002).

[16] A. Pier, K. Fehre, S. Grundmann, I. Vela-Perez, N. Strenger, M. Kircher, D. Tsitsonis, J. B. Williams, A. Senftleben, T. Baumert, M. S. Schöffler, P. V. Demekhin, F. Trinter, T. Jahnke, and R. Dörner, Chiral photoelectron angular distributions from ionization of achiral atomic and molecular species, Phys. Rev. Res. **2**, 033209 (2020).

[17] M. Tia *et al.*, Observation of enhanced chiral asymmetries in the inner-shell photoionization of uniaxially oriented methyloxirane enantiomers, J. Phys. Chem. Lett. **8**, 2780 (2017).

[18] G. Nalin *et al.*, Photoelectron circular dichroism of O 1*s*-photoelectrons of uniaxially oriented trifluoromethyloxirane: energy dependence and sensitivity to molecular configuration, Phys. Chem. Chem. Phys. **23**, 17248 (2021).

[19] K. Fehre, F. Trinter, N. M. Novikovskiy, S. Grundmann, D. Tsitsonis, S. Eckart, L. Bauer, M. Hilzinger, T. Jahnke, R. Dörner, P. V. Demekhin and M. S. Schöffler, Influence of the emission site on the photoelectron circular dichroism in trifluoromethyloxirane, Phys. Chem. Chem. Phys. **24**, 13597 (2022).

[20] K. Fehre *et al.*, A new route for enantio-sensitive structure determination by photoelectron scattering on molecules in the gas phase, Phys. Chem. Chem. Phys. **24**, 26458 (2022).

[21] K. Fehre *et al.*, Fourfold Differential Photoelectron Circular Dichroism, Phys. Rev. Lett. **127**, 103201 (2021).

[22] R. Dörner, V. Mergel, O. Jagutzki, L. Spielberger, J. Ullrich, R. Moshammer, and H. Schmidt-Böcking, Cold Target Recoil Ion Momentum Spectroscopy: a 'momentum microscope' to view atomic collision dynamics, Phys. Rep. **330**, 95 (2000).

[23] J. Ullrich, R. Moshammer, A. Dorn, R. Dörner, L. P. H. Schmidt, and H. Schmidt-Böcking, Recoil-ion and electron momentum spectroscopy: reaction-microscopes, Rep. Prog. Phys. **66**, 1463 (2003).

[24] T. Jahnke, T. Weber, T. Osipov, A. L. Landers, O. Jagutzki, L. P. H. Schmidt, C. L. Cocke, M. H. Prior, H. Schmidt-Böcking, and R. Dörner, Multicoincidence studies of photo and Auger electrons from fixed-in-space molecules using the COLTRIMS technique, J. Electron Spectrosc. Relat. Phenom. **141**, 229 (2004).

[25] K. Fehre, M. Pitzer, F. Trinter, R. Berger, A. Schießer, H. Schmidt-Böcking, R. Dörner, and M. S. Schöffler, Closed-loop recycling of rare liquid samples for gas-phase experiments, Rev. Sci. Instrum. **92**, 023205 (2021).

[26] K. Fehre, D. Trojanowskaja, J. Gatzke, M. Kunitski, F. Trinter, S. Zeller, L. P. H. Schmidt, J. Stohner, R. Berger, A. Czasch, O. Jagutzki, T. Jahnke, R. Dörner, and M. S. Schöffler, Absolute ion detection efficiencies of microchannel plates and funnel microchannel plates for multi-coincidence detection, Rev. Sci. Instrum. **89**, 045112 (2018).

[27] R. N. Zare, Photoejection dynamics, Mol. Photochem. **4**, 1 (1972).

[28] P. V. Demekhin, A. Ehresmann, and V. L. Sukhorukov, Single center method: A computational tool for ionization and electronic excitation studies of molecules, J. Chem. Phys. **134**, 024113 (2011).

[29] S. A. Galitskiy, A. N. Artemyev, K. Jänkälä, B. M. Lagutin, and P. V. Demekhin, Hartree-Fock calculation of the differential photoionization cross sections of small Li clusters, J. Chem. Phys. **142**, 034306 (2015).

[30] N. M. Novikovskiy, A. N. Artemyev, D. V. Rezvan, B. M. Lagutin, and P. V. Demekhin, Multichannel single center method, J. Phys. B: At. Mol. Opt. Phys. **55**, 175001 (2022).

[31] See Supplemental Material at http://link.aps.org/supplemental/10.1103/PhysRevResearch.5.013021 for a full account of the measured and computed MFPADs in Figs. S1–S5 and molecular-frame differential PECDs in Figs. S6–S10 for different photoelectron kinetic energies of the O 1*s* photoelectrons of *R*-TFMOx.